Magnetic Resonance in Medicine 51:331–342 (2004)

Noquist: Reduced Field-of-View Imaging by Direct Fourier Inversion

Marijn E. Brummer,[1*] David Moratal-Pérez,[2] Chung-Yi Hong,[3] Roderic I. Pettigrew,[4] José Millet-Roig,[2] and W. Thomas Dixon[5]

A novel technique called "Noquist" is introduced for the acceleration of dynamic cardiac magnetic resonance imaging (CMRI). With the use of this technique, a more sparsely sampled dynamic image sequence is reconstructed correctly, without Nyquist foldover artifact. Unlike most other reduced field-of-view (rFOV) methods, Noquist does not rely on data substitution or temporal interpolation to reconstruct the dynamic image sequence. The proposed method reduces acquisition time in dynamic MRI scans by eliminating the data redundancy associated with static regions in the dynamic scene. A reduction of imaging time is achieved by a fraction asymptotically equal to the static fraction of the FOV, by omitting acquisition of an appropriate subset of phase-encoding views from a conventional equidistant Cartesian acquisition grid. The theory behind this method is presented along with sample reconstructions from real and simulated data. Noquist is compared with conventional cine imaging by retrospective selection of a reduced data set from a full-grid conventional image sequence. In addition, a comparison is presented, using real and simulated data, of our technique with an existing rFOV technique that uses temporal interpolation. The experimental results confirm the theory, and demonstrate that Noquist reduces scan time for cine MRI while fully preserving both spatial and temporal resolution, but at the cost of a reduced signal-to-noise ratio (SNR). Magn Reson Med 51:331–342, 2004.

Key words: MRI; image reconstruction; reduced field of view; cardiac imaging; Fast cine imaging

Speed is an important factor in many dynamic magnetic resonance imaging (MRI) applications, including cardiac imaging. Time-resolved cardiac MRI (CMRI) samples the time axis by synchronizing the acquisition process with the subject's heartbeat as read from electrocardiographic or blood oximetry readings, and acquiring data at fixed intervals across the cardiac cycle. When the time sampling interval is too short to allow the acquisition of a complete spatial data set, spatial sampling is partitioned across multiple heartbeats, taking advantage of the cyclic nature of cardiac motion. Respiratory artifacts are commonly avoided by acquiring all data during breath-holding. An important limiting factor in cardiac imaging is thus the breath-hold duration that the subject can sustain. This is typically 10–25 s, depending on the patient's physical condition. Despite the growing availability of acquisition accelerators, such as parallel imaging methods (e.g., simultaneous acquisition of spatial harmonics (SMASH) (1), sensitivity encoding (SENSE) (2), and generalized autocalibrating partially parallel acquisitions (GRAPPA) (3)) on systems with phased-array RF coils, and high-speed TrueFISP steady-state acquisition techniques (4), image quality problems are still encountered that are associated with repeated breath-holding. For patients with severe cardiovascular disease, and even for healthy subjects, there are limits to both the breath-hold duration and the number of consecutive breath-hold scans that can be acquired. Faster acquisitions allow the same image to be acquired in a shorter breath-hold, higher-resolution images to be acquired in the same breath-hold time, and complete multislice coverage of anatomy to be completed in fewer breath-holds by scanning multiple slices in one breath-hold. When imaging time pushes the limits of the patient's breath-hold capacity, shorter scan times may actually improve the quality of the images. Reduced breath-hold times may improve patient throughput and result in more successfully completed studies.

One well known method for increasing the number of temporal frames in cine CMRI is view sharing (5). This temporal interpolation method, which is commercially available, reconstructs intermediate frames by combining the latter-acquired half of the data for a preceding frame with the earlier half of the data for the following frame. This approach does not change the actual temporal resolution of the scan, since the temporal acquisition window of each reconstructed frame (original or interpolated) is at least the same as that of the original uninterpolated frames. However, interpolated frames may yield sharper images in temporally undersampled situations where sudden motion occurs roughly halfway during the acquisition window of an original frame. This may improve estimations of functional parameters (e.g., the ejection fraction) at no additional cost in acquisition time.

A variety of other avenues have been pursued in the quest to reduce acquisition time in MRI. In addition to important improvements with the use of advanced hardware and faster acquisition sequences, the incorporation of various types of prior knowledge has been investigated to constrain the reconstruction problem and thus reduce data requirements. Partial-Fourier techniques (6,7), which exploit the premise that in many cases the complex-data reconstructed images are ideally expected to be real-valued, have been shown to be successful and are now available on most commercial imagers. The above-mentioned

[1]Emory University School of Medicine, Atlanta, Georgia.

[2]Universitat Politècnica de València, València, Spain.

[3]Institute of Biomedical Sciences, Academia Sinica, Taipei, Taiwan R.O.C.

[4]National Institutes of Health, Bethesda, Maryland.

[5]General Electric Global Research, Niskayuna, New York.

Grant sponsor: NIH; Grant numbers: LM06486; HL58147; Grant sponsor: Universitat Politècnica de València; Grant number: PPI-01-VIDI.

*Correspondence to: Marijn E. Brummer, Ph.D., Assistant Professor of Radiology, Department of Radiology, School of Medicine, Emory University, Atlanta, GA 30322. E-mail: mbrumme@emory.edu

Received 2 January 2003; revised 12 August 2003; accepted 15 August 2003.

DOI 10.1002/mrm.10694

Published online in Wiley InterScience (www.interscience.wiley.com).

parallel imaging methods incorporate prior knowledge about receiver coil geometry in the reconstruction of acquisitions that use phased-array receiver coils. Many other methods have been proposed to accelerate specific applications in MRI, including dynamic imaging problems. Keyhole imaging (8) exploits the observation that in many dynamic imaging problems, such as contrast uptake monitoring, intensity changes are often relatively uniform over large regions in the field of view (FOV), i.e., the dynamics are spatially band-limited. Methods such as the block regional interpolation scheme for *k*-space (BRISK) (9) and 3D time resolved imaging of contrast kinetics (TRICKS) (10) employ more elegant algorithms that have been built around this idea. The same premise is used in generalized-series reconstruction methods, such as reduced-encoding imaging with generalized-series reconstruction (RIGR) (11,12). However, cine CMRI does not align well with the underlying assumption of these types of methods, because the beating heart has an abundance of small and large anatomical structures with sharply delineated edges that may move, slowly or rapidly, in any direction within and/or through the slice plane. As a result, the dynamics of cine MRI may generally not be assumed to be band-limited in either spatial or the temporal dimensions.

An increasingly important class of methods takes advantage of the fact that dynamic imaging often involves repeated acquisitions of an image plane in which only part of the FOV changes over time. For example, in CMRI the heart moves during the cardiac cycle, but the lungs and shoulders remain in the same location. As a rule, the dynamic parts of the image contain the interesting structures in the image. Sometimes static regions provide an anatomical reference, but often the only reason for including static regions in the FOV is to avoid contamination of relevant dynamic regions by aliasing or wraparound artifacts.

Conventional dynamic MRI acquires sufficient data to reconstruct these static regions independently for each image of a time sequence. Such data are intrinsically redundant, since ideally the static region is identical in all images. A variety of modifications in data acquisition and image reconstruction have been proposed (13–20) to trade this redundancy for a reduction in acquisition time, or, alternatively, increased temporal or spatial resolution. Such acceleration techniques are known as reduced FOV (rFOV) techniques, since most proposed methods to date involve undersampled *k*-space acquisition (which corresponds to imaging with an rFOV) in combination with an approach to eliminate the resulting foldover artifact using prior knowledge of the extent and location of the dynamic portion of the FOV. A common feature of most rFOV techniques to date is the approximate amount of associated time-savings. If the size of the dynamic region represents a fraction 1/K of the total FOV, these techniques all offer scan-time reduction by a factor exactly or approximately equal to K.

Hu and Parrish (13) presented a subtraction technique whereby each frame of a dynamic sequence reconstructs a difference image with a preacquired reference image. The difference image is nonzero only in dynamic regions, and can therefore be sampled sparsely without penalty of aliasing artifact. Some practical modifications to this technique were proposed by Kyriakos et al. (14). A version for polar grid sampling was investigated by Scheffler and Hennig (15). The reference image approach is feasible for functional imaging or contrast uptake dynamics; however, full-resolution reference images are not available for cine cardiac imaging.

rFOV techniques for cardiac imaging rely on a reduction of spatial sampling density, followed by some form of temporal interpolation or filtering of the data points to eliminate foldover. Fredrickson and Pelc (16) modified the Hu and Parrish (13) approach to accommodate cyclic dynamic imaging without a preacquired full-resolution reference image. Foldover artifact is compensated for by the use of an estimated reference image, generated by averaging all acquired temporal frames. Madore et al. (17) proposed the "unaliasing by Fourier-encoding the overlaps using the temporal dimension" (UNFOLD) approach, which modulates foldover artifacts associated with spatial undersampling in predictable patterns across temporal frames. An explicit temporal filter is then applied to remove the temporal frequencies that are represented in these patterns. This method has gained attention because of its elegance and its potential applications to other problems (18,19). Recently, Madore et al. (20) proposed an rFOV approach to explicitly calculate *k*-space data that were omitted in the acquisition for a dynamic scene through the construction of difference images between frames in the dynamic image sequence. Difference images have limited FOVs and therefore are not subject to aliasing artifacts and may be reconstructed without errors from sparser samples. An explicit methodology is proposed that uses linear combinations of acquired *k*-space views and corresponding views from difference images to generate missing views from the sparse data set.

We introduce here a novel acceleration strategy we call "Noquist," which does not rely on substitution or interpolation. A more sparsely sampled dynamic image sequence is reconstructed correctly without Nyquist foldover artifact by reductions in the size of the discrete Fourier model of the *k*-space data for the dynamic image. The image is reconstructed by direct inversion of this reduced model. Our approach does not require synthesis of omitted conventional-grid data or after-the-fact removal of foldover artifacts, and accommodates variations in the dynamic FOV fraction easily and naturally.

Noquist is based on the formulation of the image reconstruction as an inverse problem. A system of simultaneous linear "data modeling" equations relates the *k*-space data to the image pixels. The image reconstruction process is defined by the inversion of this system, which is conventionally performed by an inverse discrete Fourier transform (DFT). For a unique solution on a desired image grid, the number of equations (measured data points) in the linear system must not be less than the number of variables (independent image points) to be solved in the reconstruction, as dictated by Nyquist sampling criteria. In conventional dynamic imaging, where each frame of an image sequence is reconstructed independently, these linear systems are identical for each frame of the sequence, and each frame is reconstructed from disjoint data sets by a separate DFT operation. If we know there are static regions in the FOV, the total number of independent image points that

must be computed is lower. Consequently, we can reduce the overall size of the linear system describing the sequence, and hence reconstruct the image from fewer data points. In the following we present details on the Noquist concept and our implementation.

MATERIALS AND METHODS

Theory

We will use Bracewell notation conventions (21) for the FTs. In a (static) two-dimensional (2D) MRI problem, the unknown function f we wish to reconstruct in an image is by good approximation (22) related to the measured k-space data F through an FT. For clarity, we will reduce the formulation of the image reconstruction problem to a 1D case. Imaging time constraints for a separable Cartesian 2D acquisition grid are typically dominated by sampling in the phase-encoding direction. Our technique, in its current implementation, aims to reduce the number of phase encodings. The reconstruction as described below applies to each column of the image defined by a common readout direction coordinate.

In reality, we only have access to a sampled-data version of $F(k)$. The sampling interval in k-space implicitly dictates the FOV of the image by defining the spacing between aliased copies of f in the reconstructed image. Truncation of the k-space sample train equates to application of a low-pass filter over f by capping the spatial frequency range for which data are acquired. It follows that after the k-space sampling interval and the pixel size in the reconstruction are normalized, the reconstructed image (for convenience, hereafter the function referred to as $f(x)$) is related to the sample series $F(k)$, of size N, by a DFT:

$$f(x) = \sum_{k=0}^{N-1} F(k) e^{2\pi jkx/N} \qquad [1]$$

with as inverse the "data modeling" operation:

$$F(k) = \frac{1}{N} \sum_{x=0}^{N-1} f(x) e^{-2\pi jkx/N} \qquad [2]$$

To formulate our modified reconstruction for dynamic imaging, it is convenient to rewrite the DFT relation (Eq. [2]) in vector format:

$$\vec{F} = M\vec{f} \qquad [3]$$

In Eq. [3] $\vec{F}$ is an N-dimensional vector whose elements represent the k-space data points at $k \in \{0, 1, \ldots, N-1\}$. Similarly, the vector $\vec{f}$ represents the DFT-reconstructed image at $x \in \{0, 1, \ldots, N-1\}$. The elements m_{xk} of the square data modeling matrix M contain the DFT coefficients

$$m_{xk} = \frac{1}{N} e^{-2\pi jxk/N} \qquad [4]$$

Conversely, the image reconstruction matrix M^{-1} defines the image reconstruction:

$$\vec{f} = M^{-1}\vec{F} \qquad [5]$$

and contains the inverse DFT coefficients:

$$m_{xk}^{-1} = e^{2\pi jxk/N} \qquad [6]$$

Reconstruction on a denser grid than the number of measured k-space points N can readily be shown to be equivalent to reconstruction on a grid of N points, followed by Fourier or sinc interpolation. Therefore, we will not consider such cases further in this work.

Dynamic Imaging

A complete formulation of the dynamic image reconstruction problem requires the introduction of a time variable t, thus fully defining an image by a function $f(x,t)$. Temporal sampling, like spatial sampling, is subject to Nyquist sampling criteria: sparse temporal sampling of a fast process will cause temporal aliasing effects in the time evolution of any pixel intensity. Even slow motion of sharp edges may cause step function changes in the pixel time intensity function. In reality, spatial resolution limitations may alleviate this to some degree.

We present our method under the customary assumption that the temporal sampling rate is adequate to describe the dynamics of the process being imaged, and yields a collection of k-space samples at T time points $t \in \{t_0, t_1, \ldots, t_{T-1}\}$. We modify our vector notation of the data model (Eq. [3]) and the associated image reconstruction (Eq. [5]) by adding an index τ ($0 \le \tau \le T-1$): data acquired at time t_τ are $\vec{F}_\tau$, and the reconstructed image at this time point is $\vec{f}_\tau$. The entire reconstruction problem for all T time samples may be written as a single matrix inversion by concatenating all image vectors. If

$$\vec{f} = \begin{bmatrix} \vec{f}_0 \\ \vec{f}_1 \\ \cdots \\ \vec{f}_{T-1} \end{bmatrix} \qquad [7]$$

is the image at all reconstructed time points, and

$$\vec{F} = \begin{bmatrix} \vec{F}_0 \\ \vec{F}_1 \\ \cdots \\ \vec{F}_{T-1} \end{bmatrix} \qquad [8]$$

represents the collective k-space data of the cine acquisition, the data modeling equation of the dynamic problem is again given by Eq. [3]. Similarly, the reconstruction of all frames of the entire sequence is contained in Eq. [5]. In a conventional dynamic acquisition, the same k-space sampling takes place for all frames, and thus the data modeling for any frame, represented by a submatrix M_{FRAME}, is identical to the matrix for the static case defined in Eq. [4]. The composite modeling matrix M is of

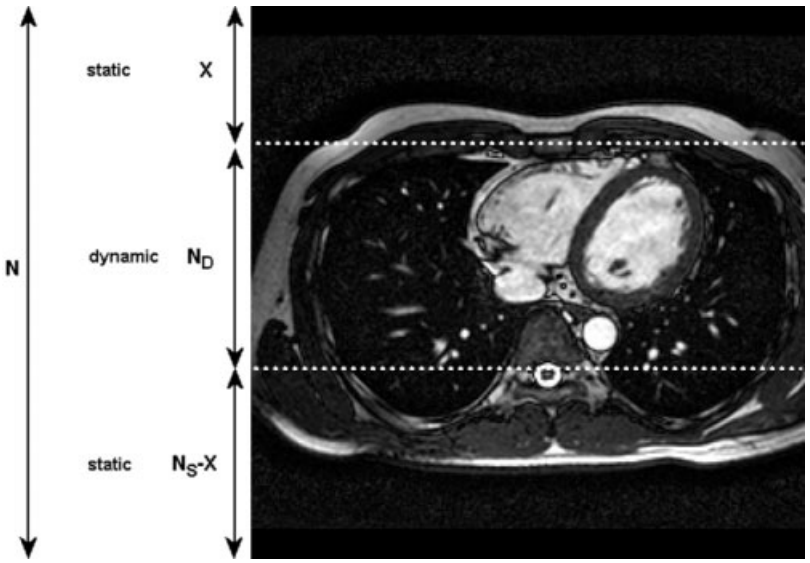

FIG. 1. Phase-encoding (vertical) FOV of size N with static region size N_S and dynamic region size N_D.

size $NT \times NT$, and is block-diagonal with identical blocks M_{FRAME} of size $N \times N$:

$$M = \begin{bmatrix} M_{FRAME} & 0 & \cdots & 0 \\ 0 & M_{FRAME} & \cdots & 0 \\ \cdots & \cdots & \cdots & \cdots \\ 0 & 0 & \cdots & M_{FRAME} \end{bmatrix} \quad [9]$$

Similarly, the reconstruction matrix M^{-1} is block-diagonal with diagonal blocks M_{FRAME}^{-1}.

Let us now consider a situation in which only part of the FOV changes over time. To take advantage of this situation, we will partition the total FOV into a "static" part with N_S points that remain unchanged throughout the dynamic scene, and a "dynamic" part with N_D points that includes at least all pixels that change in intensity during the scan (see Fig. 1). Clearly,

$$N_S + N_D = N \quad [10]$$

With prior knowledge about the approximate size and location of the static and dynamic regions, we can write each image vector $\vec{f}_\tau$ as a concatenation of a static and a dynamic image vector:

$$\vec{f}_\tau = \begin{bmatrix} \vec{f}_{\tau,S} \\ \vec{f}_{\tau,D} \end{bmatrix} \quad [11]$$

This partitioning extends into the data-modeling matrix M_{FRAME} for each time point:

$$M_{FRAME} = [\ M_S \quad M_D\ ] \quad [12]$$

where M_S is of size $N_S \times N$, and M_D of size $N_D \times N$. Since the static part of the image is identical at all points in time,

$$\vec{f}_{0,S} = \vec{f}_{1,S} = \vec{f}_{k,S} = \vec{f}_S \quad [13]$$

we may reduce the size of the dynamic image $\vec{f}$ [7] by removing duplicate elements:

$$\vec{f} = \begin{bmatrix} \vec{f}_S \\ \vec{f}_{0,D} \\ \vec{f}_{1,D} \\ \cdots \\ \vec{f}_{T-1,D} \end{bmatrix} \quad [14]$$

Accordingly, the modeling matrix (Eq. [9]) reduces to

$$M = \begin{bmatrix} M_S & M_D & 0 & \cdots & 0 \\ M_S & 0 & M_D & \cdots & 0 \\ \cdots & \cdots & \cdots & \cdots & \cdots \\ M_S & 0 & 0 & \cdots & M_D \end{bmatrix} \quad [15]$$

Acquisition of the conventional N k-space samples for each frame of the dynamic sequence thus corresponds with a modeling matrix M of size $N_{nq} \times TN$, where

$$N_{nq} = N_S + TN_D \quad [16]$$

This is an overdetermined reconstruction problem, defined by a matrix M^+ of size $TN \times N_{nq}$:

$$\vec{f} = M^+ \vec{F} \quad [17]$$

M^+ is not unique, but any valid solution satisfies the requirement

$$M^+ M = I \quad [18]$$

where I is an identity matrix of size $N_{nq} \times N_{nq}$.

Noquist Method

With the Noquist method, we reduce the data acquisition of this system to eliminate the associated data redundancy. Such a reduction in the size of $\vec{F}$ is achieved by selectively omitting acquisition of data points while retaining the critical requirement [18] that the associated data-modeling matrix M be invertible. It is clear that this requirement cannot be met if we reduce the number of data points

below the number of image points N_{nq}. We have investigated reconstruction of the image sequence with exactly this minimum data requirement, when the reconstruction matrix $M^{\dagger}$ is uniquely defined ($M^{\dagger} = M^{-1}$). This implies the acquisition of

$$N_{frame} = N_{nq}/T = N_D + N_S/T \qquad [19]$$

samples per frame. Note that this minimum number of data points for a fully determined reconstruction problem is slightly larger than the number typically advocated for rFOV methods. All of the published methods to date pursue reconstruction from N_D samples per frame (13–20).

Data Selection

It is important to select an appropriate subset of N_{frame} *k*-space views out of *N* for each frame. The total number of possible selections can be quite large. For example, in an acquisition with $N = 256$ phase encodings, $T = 16$ temporal frames, and half of the FOV dynamic ($N_D = N_S = 128$), we must select $N_{frame} = 136$ out of 256 data points for each temporal frame. The number of choices for each frame is the number of combinations of N_{frame} from N samples, totaling for all frames:

$$\left(\begin{array}{c} N_{frame} \\ N \end{array} \right)^T = \left(\frac{256!}{136!120!} \right)^{16} = 5.18 \times 10^{1208} \qquad [20]$$

Quite a few of these many possible selections will yield a nonsingular matrix *M*, and thus present a feasible choice. The selection of *k*-space views determines the condition of the reconstruction problem, quantified by the condition number (23) of the data-modeling matrix *M*. We have designed and experimented with several heuristic algorithms for the selection of an appropriate subset of *k*-space data points. Our algorithms were based upon the conjecture that for stability the sampling grid should ideally be uniformly dense across the entire FOV in (*k,t*)-space. To date, we have not addressed optimization with respect to noise propagation or other image characteristics.

Presented below are some examples of data-selection algorithms, for a case of 50% static FOV:

1. All even *k*-space lines are acquired in every frame, and odd *k*-space lines in interlaced evenly spaced patterns (see Fig. 2a). This algorithm is guaranteed to sample each phase-encoding at least once, which is a necessary condition for a nonsingular modeling matrix (Eq. [15]). Other criteria that led to this choice are symmetry in *k*-space coverage, guaranteed small maximum spacing between *k*-space samples, and simplicity of the selection algorithm.
2. All even *k*-space lines are acquired in all even frames, and odd *k*-space lines are sampled once each, distributed across frames and *k*-space at interlaced evenly-spaced patterns. All odd *k*-space lines in all odd frames, and even *k*-space lines, are acquired once each in interlaced evenly-spaced patterns (see Fig. 2b). This algorithm is similar to algorithm 1, with the additional characteristic that (for an even number of frames) all *k*-space lines are sampled an equal number of times.
3. The desired number of lines is randomly selected in every frame (see Fig. 2c). Although a random choice carries the risk of generating a singular modeling matrix (Eq. [15]) because there is a nonzero probability that one or more *k*-space grid points are not acquired at any time sample point, it has the potential advantage of reducing correlated noise in the reconstruction that is associated with symmetric sampling grids.

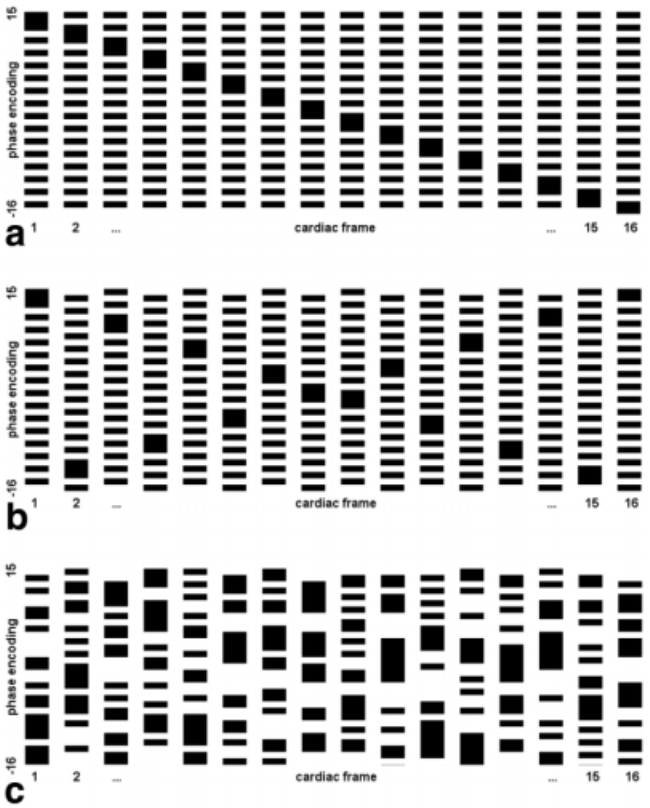

FIG. 2. *k*-Space sampling grid selection algorithms for a 32-view, 16-frame Noquist acquisition with 50% static FOV ($N_{frame} = 17$). Black lines indicate acquired data, white lines indicate omitted data, and solid black columns represent conventional acquisition. **a:** Algorithm 1. All even phase encodings are acquired in every phase, and all odd encodings are acquired once, evenly spaced across the *k*-space FOV and staggered across cardiac phases. This algorithm yields a data modeling matrix *M* with reciprocal condition number $L = 4.32\text{e-}04$. **b:** Algorithm 2. All even phase encodings are acquired in every even phase, with odd encodings evenly spaced across the *k*-space FOV. All odd encodings are acquired in every odd phase, with the even encodings evenly spaced across the *k*-space FOV. This algorithm generates a data modeling matrix with $L = 3.06\text{e-}04$. **c:** Algorithm 3. Data lines are selected randomly, constrained by the requirement that all views be selected at least once in the entire sequence. This algorithm generates a data modeling matrix condition number that varies with the realization of the random process. The combination shown had a relatively ill-conditioned matrix *M* with $L = 3.13\text{e-}06$.

These heuristic algorithms readily extend to a variety of image sizes *N* and different dynamic region sizes N_D. For

any given sampling grid size and static fraction, many phase-encoding view subset selections result in an invertible modeling matrix M, from which the image may be reconstructed. An important quality measure for data-selection algorithms is noise propagation into the reconstructed image.

Stability and Noise Propagation

The condition of the data-modeling matrix defines the propagation of data noise into the reconstructed image. Assuming a constant noise level during k-space acquisition, all elements of the data vector $\vec{F}$ will have an identically and normally distributed zero-mean uncorrelated complex-data noise term v defined by the standard deviation σ. A pixel in the image with phase-encoding direction coordinate x in the image vector $\hat{f}$ is reconstructed by a linear system M^{-1} (with matrix elements m_{xk}^{-1}):

$$f(x) = \sum_{k=0}^{N_{nq}-1} m_{xk}^{-1} F(k) \qquad [21]$$

The noise terms $v(k)$ in the measured data $\hat{F}(k) = F(k) + v(k)$ propagate into image noise $\phi(x)$ by

$$\hat{f}(x) = \sum_{k=0}^{N_{nq}-1} m_{xk}^{-1}\hat{F}(k) = f(x) + \sum_{k=0}^{N_{nq}-1} m_{xk}^{-1} v(k) = f(x) + \phi(x) \qquad [22]$$

Since ϕ_x is a linear combination of normally distributed random variables, it is also a normally distributed white noise term, with variance $Var\{\phi(x)\}$:

$$Var\{\phi(x)\} = \sigma^2 \sum_{k=0}^{N_{nq}-1} |m_{xk}^{-1}|^2 \qquad [23]$$

Compare this expression to the noise variance of conventional DFT reconstruction to quantify the differences in noise propagation. In conventional reconstruction, an expression analogous to Eq. [22] can be formulated for each individual temporal frame:

$$\hat{f}_{DFT}(x) = \sum_{k=0}^{N-1} m_{xk}^{-1}\hat{F}(k) = f(x) + \sum_{k=0}^{N-1} m_{xk}^{-1} v(k) = f(x) + \phi_{DFT}(x) \qquad [24]$$

In this case, the reconstruction matrix elements $m^{-1}{}_{xk}$ are the inverse DFT coefficients (Eq. [6]). These all have a magnitude of one, so the equivalent noise variance for DFT reconstruction is

$$Var\{\phi_{DFT}(x)\} = \sigma^2 \sum_{k=0}^{N-1} |m_{xk}^{-1}|^2 = \sigma^2 \sum_{k=0}^{N-1} |e^{2\pi jxk/N}|^2 = N\sigma^2 \qquad [25]$$

Equations [23] and [25] allow us to calculate a linear noise amplification factor $\Phi(x)$ for Noquist reconstruction at location x, relative to DFT reconstruction, independently of the signal-to-noise ratio (SNR) of the data and the contents of the image:

$$\Phi(x) = \sqrt{\frac{Var\{\phi(x)\}}{Var\{\phi_{DFT}(x)\}}} = \sqrt{\frac{1}{N}\sum_{k=0}^{N_{nq}-1} |m_{xk}^{-1}|^2} \qquad [26]$$

Optimization with respect to this quantity of the data-selection algorithm will be pursued in a follow-up investigation. However, the current results show that even before such optimized data selection is fully understood or available, the Noquist method may be applied with stable results using ad hoc view selection method 1.

Experimental Methods

Experiments were designed to test the Noquist method using simulation phantom data and actual MRI data. We also compared Noquist with the UNFOLD method (17), a promising rFOV technique that employs temporal filtering. All simulations and reconstructions were implemented in MATLAB V6.1 (MathWorks, Inc., Natick, MA). Calculations were performed in complex-data format, fully preserving phase information in k-space and image space.

Phantom Simulation Data

A 2D simulation phantom data set was designed to reflect overall image structure in an axial MRI image of the heart. The phantom data were generated in a sampled k-space representation. This was achieved by designing the 2D frames of the phantom image sequence as a linear superposition of elliptical objects, whose FTs were scaled "*jinc*" functions ($jinc\ x = J_1(\pi x)/(2x)$, where J_1 is a first-order Bessel function) (20), and whose k-space samples could thus be evaluated directly. As a result, the phantom simulates realistic k-space sampling and truncation. Idealized temporal sampling of the cardiac cycle was simulated (i.e., the cycle was sampled at 16 equidistant time points with an infinitely short readout interval).

The dynamics of the phantom image sequence simulate different elementary types of cardiac-synchronous motion. The phantom image sequence (see Fig. 3 for systolic and diastolic frame images) has a static background object simulating an axial view through the thorax. It contains five objects in the central half of the FOV that simulate different types of motion, which may be encountered in breath-hold CMRI. The phantom data set was generated on a 256×256 spatial sampling grid, with 16 temporal frames. Reconstructions were obtained from both noiseless and noisy data. Normally distributed white noise with 16dB SNR was added to the complex k-space data.

Reduced data sets for the Noquist and UNFOLD reconstructions were simulated by selection of appropriate subsets of phase-encoding views ("horizontal lines") from the k-space data.

MRI Data

Raw data (i.e., before reconstruction) were collected with breath-held vector-cardiogram-gated cine-imaging se-

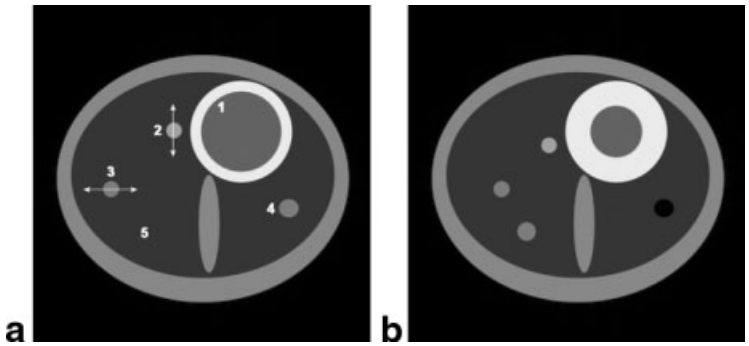

FIG. 3. Frames 1 (**a:** diastole) and 7 (**b:** systole) of 16 in a 256 × 256-pixel phantom image sequence. The phantom was designed to reflect overall structure in an axial slice through the thorax, with features simulating different types of cardiac-synchronous motion that may be encountered in CMRI. All moving objects are located in the center half of the vertical (phase-encoding) FOV. They include simulated left ventricular contraction (bright annulus 1) with dynamics derived from measured values in a short-axis movie of a healthy volunteer, circles undergoing sinusoidal translational vertical (2) and horizontal (3) motion, sinusoidal intensity variation across the cardiac cycle (circle 4), and single-frame flash intensity changes (circle 5), which only differs from the background intensity in frame 7.

quences of the heart in patients and normal volunteers. The MRI data shown in the illustrations were all acquired on a 1.5T Philips Gyroscan Intera scanner (software release 7.1.2; Philips Medical Systems, Inc.) using a balanced fast field echo (bFFE) steady-state free precession (SSFP) sequence and a five-element phased-array receiver coil designed for cardiac applications. Typical parameters were 192–256 phase encodings, TR = 3.5 ms, TE = 1.7 ms, flip angle = 60 degrees, FOV = 250–350 mm with 2× readout oversampling, and 12–24 frames per cardiac cycle.

Noquist Reconstruction

Data modeling matrices were generated following the data subset selection algorithms discussed in the Theory section above. Since rFOV data reduction was applied retrospectively, full-grid data sets were available in all cases. Knowledge about the location and size of the static fraction of the FOV was derived from observations from full-grid reconstructions. The data-modeling matrix M was calculated according to Eq. [15]. Data-selection algorithm 1 was used in all reconstructions shown. Matrix inversion was performed to yield a reconstruction matrix, which was applied to the data column associated with each pixel along the frequency-encoding axis.

RESULTS AND DISCUSSION

Noiseless Phantom Data

For simulation phantom data without added noise, the first three images in Fig. 4 compare Noquist reconstruction with conventional reconstructions from full-grid data, and with zero-padded, low frequency-only, reduced data with equal hypothetical acquisition time. Note that for the noiseless data, Noquist is an analytic equivalent of full-grid FFT reconstruction if the rFOV requirement is satisfied. In the case of our noiseless simulated k-space data, this is compromised only by the Gibbs' phenomenon near moving edges due to truncation of the sample train, which causes ringing artifacts that extend beyond the assumed static region boundary. In Fig. 4, where the boundary of the dynamic region was defined several pixels away from moving edges, the resulting differences between Noquist reconstruction and full-grid FFT reconstruction were below detection in the 256-gray-level dynamic range of the figure. The reduced-data conventional image (Fig. 4c), which uses the exact same number of data points as Noquist, shows marked degradation by Gibbs' ringing artifact due to the absence of high-spatial-frequency data.

Noise Propagation in Phantom Data

The same phantom and resolution characteristics, but now with normally distributed white noise (SNR = 16 dB) added to the complex k-space data, are presented in Fig. 4d–f. The Noquist reconstruction (Fig. 4e) illustrates the price paid for accelerated acquisition by Noquist. Again, the spatial and temporal resolution are fully preserved, but the noise level in the dynamic region is higher than in the same region in the conventional image. The noise level is not constant across the image, and as a rule is higher in the dynamic FOV. Table 1 confirms that there is a good correspondence between theoretical noise propagation following Eq. [26] and observations from phantom reconstructions by the three data-selection methods discussed in the previous section. Noise SDs were measured in manually defined regions in the medium-gray outer ellipse of the phantom object that mimics skin (static) and in the blood pool inside the myocardium object (dynamic) in modulus reconstructions (scaled to the integer in the range [0, 255]). Selection methods 1 and 2 performed comparably, with method 1 generally yielding slightly better results. For this reason, all results were generated using this selection algorithm. Noise levels in static regions by Noquist using method 1 (well-conditioned data modeling matrix) are approximately equal to those in conventional FFT reconstructions.

For an ill-conditioned data modeling matrix M, as observed in a series of six realizations of Noquist with random phase-encoding view selection (method 3), the reconstruction matrix M^{-1} may show very large absolute values of m_{xk} in dynamic regions, resulting in high local noise amplification [26]. Noquist using selection method 3 consistently performed poorly with very high local noise am-

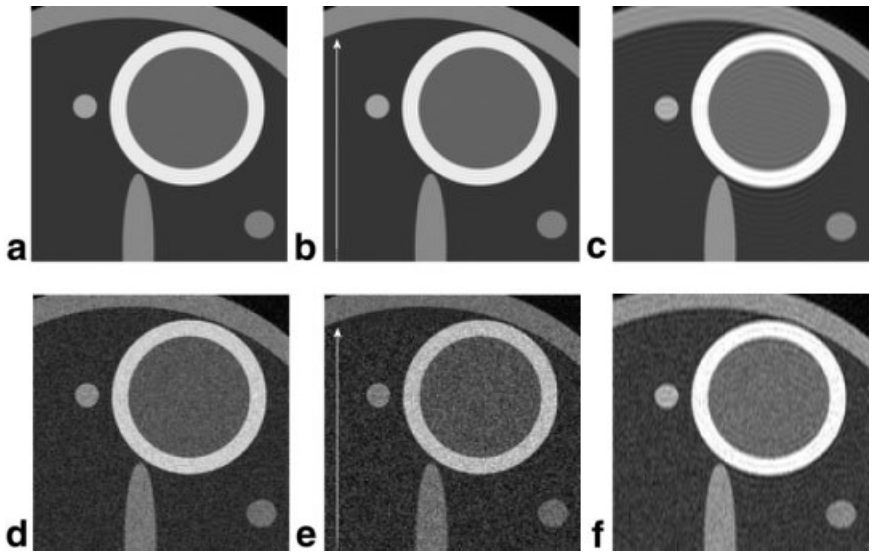

FIG. 4. Central cropped portion of the first of 16 frames (See Figure 3a for entire phantom image) of phantom object reconstructions with 256×256 image grid from 256 simulated phase-encodings. The center half of the vertical FOV (indicated by arrows in (**b**) and (**e**)) is considered dynamic for Noquist. Images (a–c) show results from noiseless *k*-space data: (**a**) Full-grid conventional reconstruction; (**b**) Noquist reduced-data reconstruction from 53% of the data selected by algorithm 1 (see text); (**c**) Reduced-data conventional reconstruction from the central 53% of the *k*-space data (136 of 256 phase encodings). Images (**b**) and (**c**) have equal hypothetical acquisition times. Images (**d-f**) show the same comparison with 16dB normally distributed white noise added to the complex *k*-space data. Dynamic regions in the NoQuist reconstruction have a different noise level from static regions.

plification, resulting in noise-drowned images that were unsuitable for measuring noise statistics.

These results emphasize the importance of choosing a favorable Noquist selection algorithm. Optimization of data selection, based on earlier research on optimized *k*-space sampling based on criteria from information theory (24,25) or further prior knowledge about local intensity characteristics (26), will be an important next step in further investigations. However, the results in the following sections underline our earlier point that even before such optimization of parameters with respect to SNR, stable Noquist reconstructions can be consistently obtained by ad hoc data selection method 1, which is used in all of the following figures.

Transverse MRI Images

Figure 5 makes the same comparison as Fig. 4 but shows a human image, with the same result. The conventional reduced-data reconstruction shows substantial loss of image detail due to absence of high-spatial-frequency data. Edge details are fully preserved in the Noquist reconstruction.

Short-Axis Image

Figure 6 shows Noquist reconstructions of a short-axis slice through the heart of a normal volunteer. Compared to the conventional full-grid reconstruction, Noquist reconstructions with increasing data reduction faithfully preserve image detail, with decreasing SNR. The image in Fig. 6e, which uses only 25% of the data, still shows adequate SNR for evaluation of myocardial functional parameters such as ejection fraction and radial thickening. In this image, which has the greatest data reduction, the heart, but not the descending aorta, lies inside the region classified as dynamic for Noquist. Therefore the aorta, but not the heart, causes a column of ghost artifacts. Even so, such ghost artifact columns can be oriented away from the areas of interest by an appropriate choice of the phase-encoding direction. The reduced-data image may still have undi-

Table 1
Noise Characteristics in Phantom Data (See Fig. 4) Reconstructions by FFT and Noquist

Reconstruction method	Region	Mean intensity (±SD σ)	Scaled σ	Noise propagation factor per (26)	Inverse condition number of *M*
Full-grid FFT	Blood pool	91.99 (±6.76)	1.0000	–	
Noquist (algorithm 1)	Skin (static)	118.75 (±6.37)	0.9998	1.0000	5.4066e−05
Noquist (algorithm 1)	Blood pool (dynamic)	86.8 (±9.65)	1.5128	1.6955	5.4066e−05
Noquist (algorithm 2)	Skin (static)	116.78 (±8.61)	1.3644	1.4142	3.823e−5
Noquist (algorithm 2)	Blood pool (dynamic)	85.87 (±11.26)	1.7652	1.9685	3.823e−5
Noquist (algorithm 3)	–	–	–	7.00e+09 (mean of 6 experiments)	3.74e−16

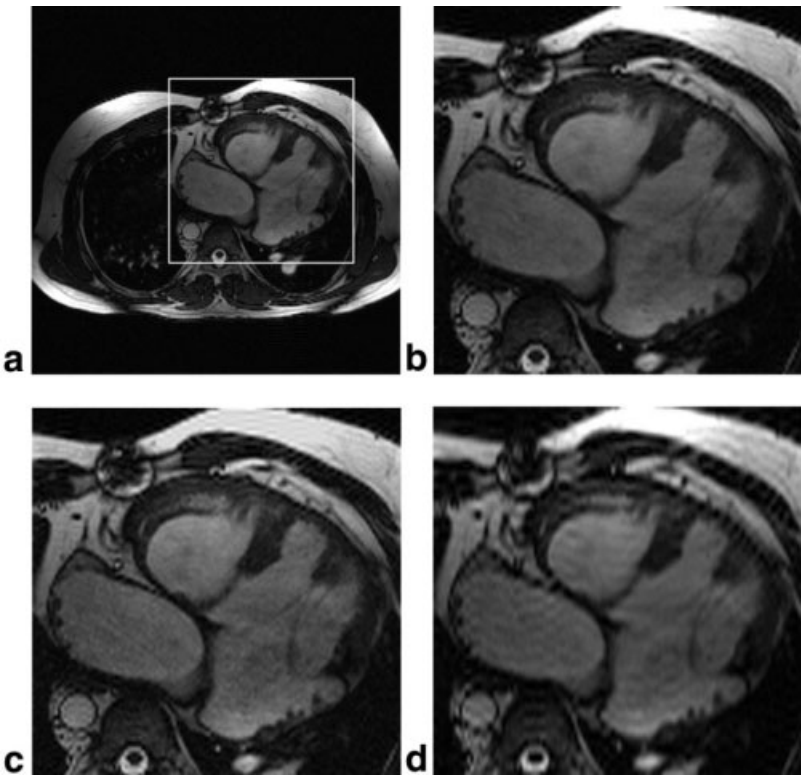

FIG. 5. First of 12 frames in an axial bFFE movie with a 256 × 256 image grid from 192 phase-encodings. The center 50% of the FOV is treated as dynamic for Noquist. **a:** Full-grid conventional reconstruction at full FOV. **b:** The same image cropped to a region showing the heart. **c:** Noquist reduced-data reconstruction using 54% of the data (104 of 192 phase encodings per frame). **d:** Conventional reconstruction from the same number of phase-encoding views as the Noquist reconstruction (**c**), using only the central portion of the acquired *k*-space data. Images **c** and **d** have equal hypothetical acquisition times.

minished diagnostic value despite a 75% reduction in acquisition time.

Comparison With UNFOLD

Figure 7 compares, using the noiseless phantom data, (a) conventional, full-grid reconstruction; (b) Noquist from $N_{frame} = 128 + 128/16 = 136$ phase-encodings per temporal frame; and (c) UNFOLD from 128 phase-encodings per temporal frame, implemented as proposed in Ref. 17. The UNFOLD reconstruction shows the side effects of the temporal filter it employs. Cross-talk between temporal frames due to sidelobes in the point spread function of the temporal Fermi filter results in ghost artifacts showing the location of moving objects in frames both preceding and following each frame. Of the five moving objects in the phantom image, only the dynamics of the stationary object with sinusoidal intensity variation (number 4 in Fig. 3) is reconstructed without artifact by UNFOLD. Using marginally more data, Noquist reconstructs dynamics faithfully.

Similar observations may be made in the same comparison on actual MRI data. Noquist and UNFOLD reconstructions of a vertical long-axis image are shown in Fig. 8. The UNFOLD reconstruction has higher SNR, but Noquist preserves edge detail better. We can observe this most clearly in the (amplified) absolute difference images, where discrepancies between the full-grid and reduced-data reconstructions are diffuse across the entire region for Noquist (Fig. 8e), but are concentrated at the edges of moving objects for UNFOLD (Fig. 8f).

Computational Aspects

Reconstruction by Noquist replaces efficient FFT inversion by direct inversion through straightforward matrix multiplication. In addition, unlike conventional reconstruction, the time and phase-encoding dimensions are no longer separable, since the static region is shared between all frames. As a result, an increased computational burden is associated with the Noquist approach. In our implementation, where reconstruction in the readout direction is performed by FFT, only the phase-encoding reconstruction is affected. Let us consider a cine sequence of T images of size $N \times N$, and let us ignore in this analysis the readout FFT reconstruction altogether, since it is the same in both cases. Conventional phase-encoding FFT reconstruction for all N readout pixels and all T time frames of the entire cine series requires a number of complex multiplications C_{FFT} equal to:

$$C_{FFT} = TN(N \log N) \qquad [27]$$

Noquist reconstruction requires C_{nq} complex operations for the reconstruction:

$$C_{nq} = N(N_{nq})^2 = N(N_S + TN_D)^2 \qquad [28]$$

Conventional (phase-encoding) FFT reconstruction of a cine sequence thus involves an algorithm of order $TN^2 \log N$, and Noquist reconstruction is an algorithm of order T^2N^3. For realistic dimensions such as $N = 256$, $T = 16$, and a 50% dynamic FOV, FFT phase-encoding reconstruction requires 8 million complex floating-point operations. Noquist reconstruction requires 1.2 billion operations, or about a factor of 144 more.

We note that although the $N_{nq} \times N_{nq}$ matrix inversion, which is required to obtain reconstruction matrix M^{-1}, is a computationally intensive operation, it can be precom-

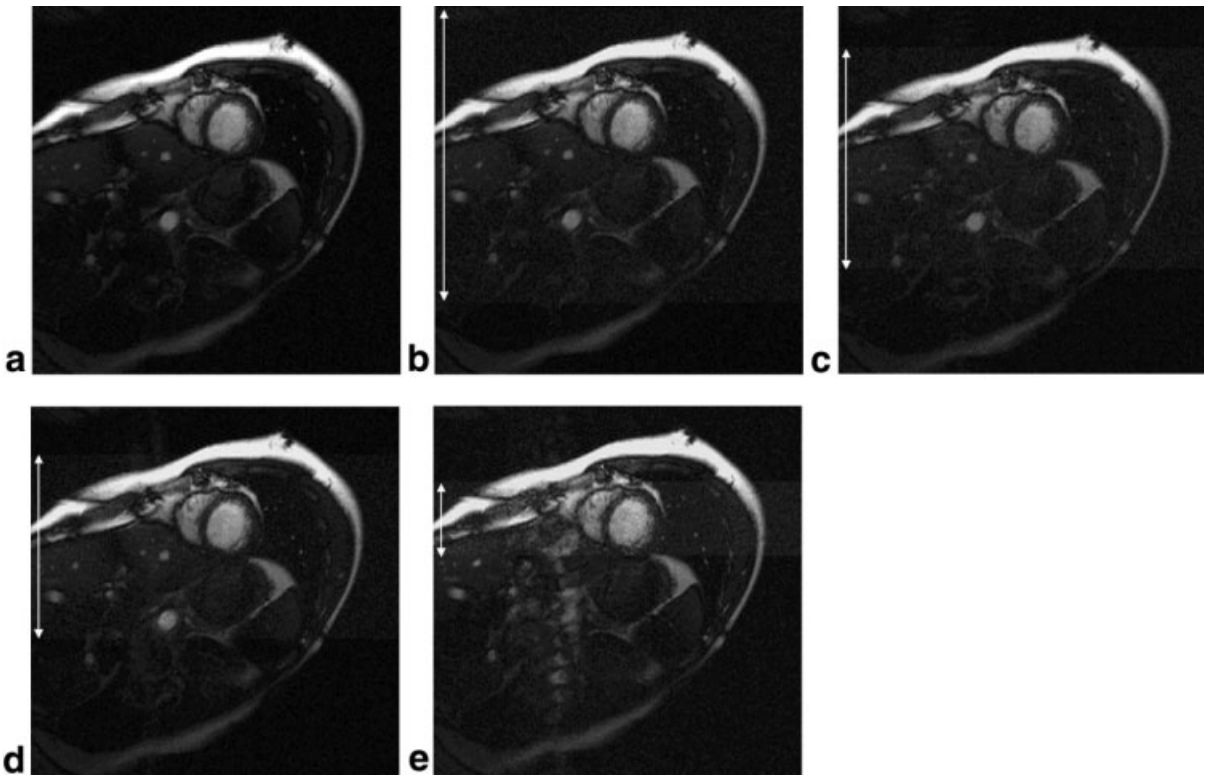

FIG. 6. First of 16 frames in a short-axis study, acquired using four elements of a phased-array coil, with 160 phase-encoding views per frame. Phase encoding is vertical. **a:** A 256 × 256 conventional FFT reconstruction. **b–e:** Noquist reconstructions with increasing levels of data reduction (arrows indicate the extent of the dynamic region): (**b**) 80% dynamic FOV, with $N_{frame} = 130$ or 18.75% data reduction; (**c**) 60% dynamic FOV, with $N_{frame} = 100$ or 37.5% data reduction; (**d**) 50% static FOV, with $N_{frame} = 85$ or 46.9% data reduction; and (**e**) 20% dynamic FOV, with $N_{frame} = 40$ or 75% data reduction.

puted. For a given spatial and temporal resolution, the matrix elements do not depend on the location of the static portion of the FOV. For example, a practical reconstruction system may be designed to expect the static FOV at the top of the image, and apply an image wrap operation to ensure compliance with this requirement before the reconstruction (Eq. [17]) is evaluated. A manageable database of precomputed reconstruction matrices for a range of dynamic FOV fractions and resolution parameters may be stored in the image reconstruction system. If a matrix is required of different dimensions from those found on the system, it must be calculated once, to be subsequently stored and incorporated in the database. We note that for a given number of frames, only a different *size* of the dynamic region may require calculation of a new reconstruction matrix. The same matrix will accommodate any *location* of the dynamic region through a cyclic image wrap, or alternatively linear phase warping in k-space.

We timed reconstructions by MATLAB on a 1.4GHz Dell Dimension 8100 with 1Gb of PC800 RAM. Conventional phase-encoding FFT reconstruction of a complete 16-frame cardiac movie with 256 phase encodings of 512 readout samples required 1.15 s. The Noquist direct matrix multiplication for 128 static and 128 dynamic pixels (reconstruction matrix $M^{-1} = 2176 \times 2176$) required 22.9 s, or a factor of 20 higher than FFT reconstruction. This is less than what we expected from the above analysis by numbers of complex multiplications, possibly indicating high

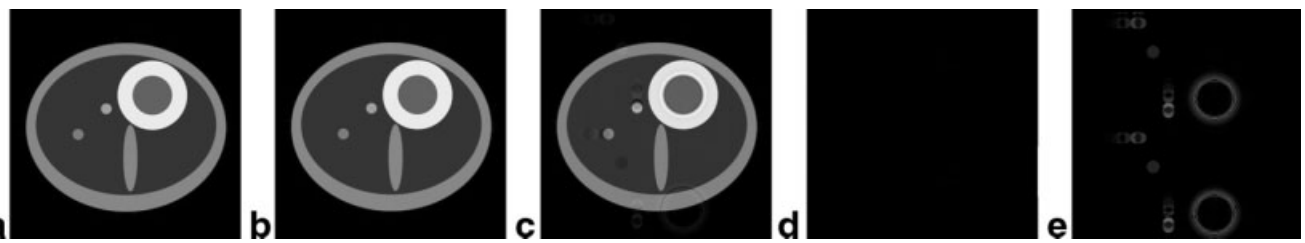

FIG. 7. Frame 5 of 16 from phantom object reconstructions from noiseless data with a 256 × 256 image grid from 256 simulated phase encodings. **a:** Full-grid conventional reconstruction. **b:** Noquist reconstruction (identical to **b**). **c:** UNFOLD reconstruction. The ghost artifacts of the moving objects are a result of the temporal filtering employed in this technique. **d** and **e:** Absolute difference images of the reduced-data reconstructions (**b** and **c**) and the full-resolution reconstruction (**a**), with intensities amplified by a factor of 4 for visibility.

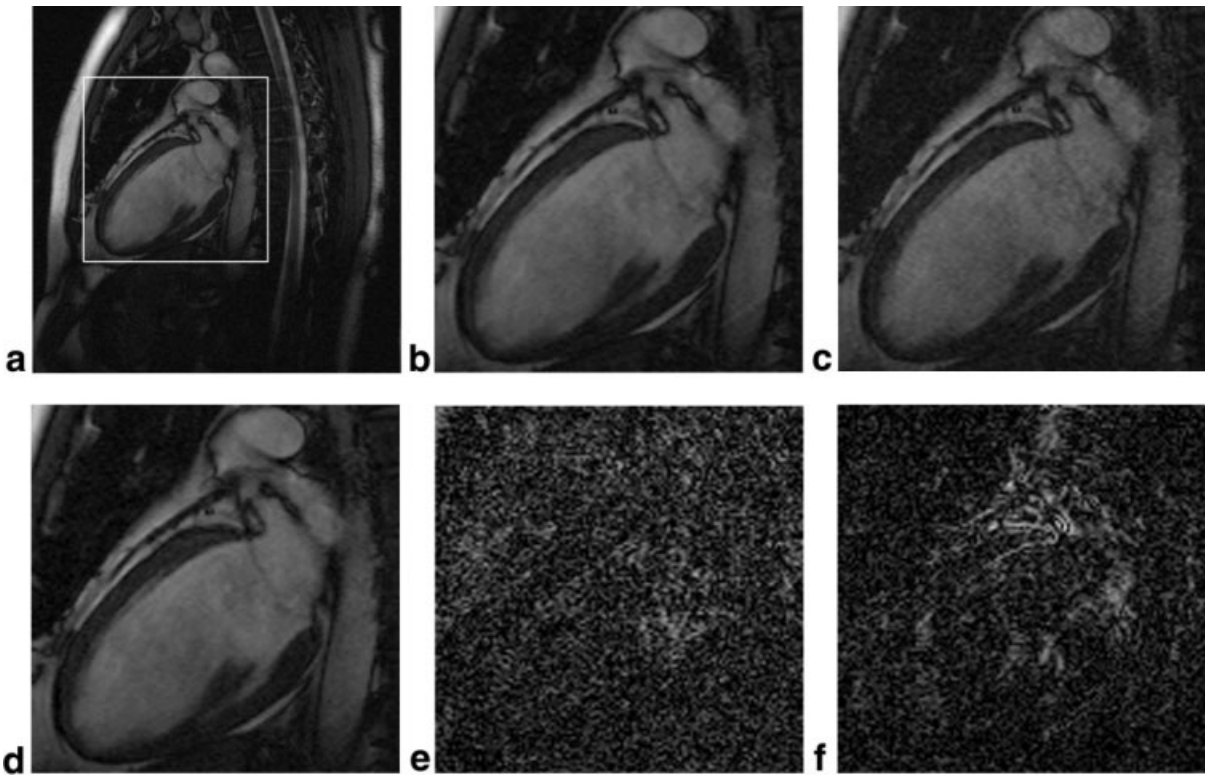

FIG. 8. First of 16 frames of a cine acquisition from 256 phase encodings: (**a**) conventional full-grid reconstruction, (**b**) magnified by a factor of 2 and cropped to the heart region; (**c**) Noquist and (**d**) UNFOLD, both with 50% static FOV. Absolute difference between full-resolution and (**e**) Noquist or (**f**) UNFOLD reconstructions, amplified by a factor of 8 for visibility.

numerical efficiency of simple matrix multiplications on this hardware. The inversion of the 2176×2176 modeling matrix required approximately 101 s.

Generalization and Considerations for Improvement

Our implementation of Noquist achieves a gain in acquisition time by considering static FOV redundancy in the phase-encoding dimension alone. Conceptually, the method extends readily to further efficiency gains by also taking into consideration static portions of the FOV in the readout direction. Practical implementation of this generalization will require reformulation of the complete 2D reconstruction problem by direct Fourier inversion. The size of the reconstruction matrix for resolutions desired in clinical CMRI may still become large for current capabilities of practical image reconstruction hardware. The same may apply to the application of Noquist in nonseparable, non-Cartesian imaging techniques, such as spiral acquisition trajectories. However, we know of no theoretical barriers that would preclude the use of Noquist in such situations, or in conjunction with other accelerators (e.g., parallel imaging).

Apart from applications in structural CMRI, the proposed technique has the potential to expand the scope of quantitative blood flow (QF) measurements by MRI. High-resolution phase velocity imaging in breath-hold mode in the chest and abdomen currently requires very long breath-hold times on current-generation MRI equipment. The ability to reduce scan time without sacrificing resolution may greatly improve the success rate and reliability of breath-hold QF studies. In particular, when derived parameters (such as vessel compliance) that are sensitive to accurate estimations of the vessel boundary location are sought, Noquist may become the rFOV method of choice, since methods that use temporal interpolation introduce edge blurring.

In principle, Noquist does not require the dynamic FOV to be contiguous. This observation may be of particular interest for flow imaging, where there may be no motion of large contiguous organs, but only motion by intensity changes in several blood vessels that appear in disjoint locations in the FOV, with static regions in between. The use of Noquist reconstruction in such a situation may require a different reconstruction matrix than the contiguous case, but the data reduction is the same as for a contiguous dynamic FOV of the same accumulated size. By a similar argument, it is also possible to subsequently correct (based on findings from an initial Noquist reconstruction) the location, but not the size, of the dynamic FOV in a reduced-data acquisition, and repeat the reconstruction without requiring new data.

Optimization of data selection with respect to noise propagation is an issue that is still under investigation. Although our current implementation has yielded stable results in all experimental data sets to date, a better understanding of the reconstruction matrix properties may produce further improvements in SNR with no additional cost in acquisition time or computational load.

We currently perform Noquist reconstruction by straightforward matrix multiplication. The reconstruction matrix M^{-1} is the inverse of a block-diagonal matrix with a high degree of symmetry. We have observed that many reconstruction matrices show ordered patterns, sometimes with large groups of identical elements. It may be possible to exploit this feature for the design of more efficient image-reconstruction algorithms—for example, by changing the order of addition and multiplication at critical points.

CONCLUSIONS

The proposed Noquist method reduces acquisition time in dynamic MRI scans by eliminating the data redundancy associated with static regions in the dynamic scene. A reduction of acquisition time is achieved, asymptotically equal to the static fraction of the FOV, by omitting the acquisition of a strategically selected subset of phase-encoding views from a conventional equidistant Cartesian acquisition grid. The method works with MRI data of any orientation or pulse sequence, with stable image intensity characteristics across the frames in the dynamic sequence. Phantom studies demonstrate that this technique can reconstruct an image sequence with full preservation of both spatial and temporal resolution, using only a fraction of the data. rFOV techniques that use temporal filtering can not do this. In addition, our method allows more flexibility in the dynamic fraction of the FOV than previously proposed methods that use temporal filtering. The cost is a reduction in SNR (which is most important in the dynamic region of the image) that depends on the condition of the reconstruction matrix as determined by the selection of a subset of data from the full Cartesian acquisition grid.

The Noquist method also adds to the computational burden of image reconstruction. Efficient implementation of this method on an imaging instrument may involve storing precomputed reconstruction matrix coefficients for an array of spatial and temporal scan dimensions to avoid having to perform a matrix inversion for each scan. The user interface for scan preparation must allow interactive definition of the location and size of the static and dynamic FOV regions.

The proposed method can be implemented immediately with most of the imaging equipment available today, without additional acquisition hardware. Optimization of data subset selections may yield further SNR improvements. The method is also promising as a means of accelerating phase velocity-encoded imaging for quantitative flow mapping.

ACKNOWLEDGMENTS

The authors thank John Oshinski and Puneet Sharma for their expert help with data acquisition.

REFERENCES

1. Sodickson DK, Manning WJ. Simultaneous acquisition of spatial harmonics (SMASH): fast imaging with radiofrequency coil arrays. Magn Reson Med 1997;38:591–603.
2. Pruessmann KP, Weiger M, Scheidegger MB, Boesiger P. SENSE: sensitivity encoding for fast MRI. Magn Reson Med 1999;42:952–962.
3. Griswold MA, R. Heidemann R, Nittka M, Jellus V, Wang J, Haase A, Jakob PM. Generalized auto-calibrating partially parallel acquisitions (GRAPPA). Magn Reson Med 2002;47:1202–1210.
4. Oppelt A, Graumann R, Barfuβ H, Fischer H, Hartl W, Schajor W. FISP—a new fast MRI sequence. Electromedica (Engl Ed) 1986;54:15–18.
5. Foo TK, Bernstein MA, Aisen AM, Hernandez RJ, Collick BD, Bernstein T. Improved ejection fraction and flow velocity estimates with use of view sharing and uniform repetition time excitation with fast cardiac techniques. Radiology 1995;195:471–478.
6. Feinberg DA, Hale JD, Watts JC, Kaufman L, Mark A. Halving MR imaging time by conjugation: demonstration at 3.5 kG. Radiology 1986; 161:527–531.
7. Margosian P, Schmitt F, Purdy DE. Faster MR imaging: imaging with half the data. Healthcare Instr 1986;1:195–197.
8. Vaals JJ Van, Brummer ME, Dixon WT, Tuithof HH, Engels H, Nelson RC, Gerety BM, Chezmar JL, Den Boer JA. "Keyhole" method for accelerating imaging of contrast uptake. J Magn Reson Imaging 1993;3:671–675.
9. Doyle M, Walsh EG, Blackwell GG, Pohost GM. Block-regional interpolation scheme for k-space (BRISK): a rapid cardiac imaging technique. Magn Reson Med 1995;33:163–170.
10. Korosec FR, Frayne R, Grist TM, Mistretta CA. Time-resolved contrast-enhanced 3D MR angiography. Magn Reson Med 1996;36:345–351.
11. Liang ZP, Lauterbur PC. A generalized series approach to MR spectroscopic imaging. IEEE Trans Med Imaging 1991;10:132–137.
12. Webb A, Liang ZP, Magin RL, Lauterbur PC. Application of reduced encoding MR imaging with generalized series reconstruction (RIGR). J Magn Reson Imaging 1993;3:925–928.
13. Hu X, Parrish T. Reduction of field of view for dynamic imaging. Magn Reson Med 1994;31:691–694.
14. Kyriakos WE, Panych LP, Zientara GP, Jolesz FA. Implementation of a reduced field-of-view method for dynamic MR imaging using navigator echoes. J Magn Reson Imaging 1997;7:376–381.
15. Scheffler K, Hennig J. Reduced circular field-of-view imaging. Magn Reson Med 1998;40:474–480.
16. Fredrickson JO, Pelc NJ. Temporal resolution improvement in dynamic imaging. Magn Reson Med 1996;35:621–625.
17. Madore B, Glover GH, Pelc NJ. Unaliasing by Fourier-encoding the overlaps using the temporal dimension (UNFOLD), applied to cardiac imaging and fMRI. Magn Reson Med 1999;42:813–828.
18. Madore B. Using UNFOLD to remove artifacts in dynamic imaging. In: Proceedings of the 9th Annual Meeting of ISMRM, Glasgow, Scotland, 2001.
19. Madore B. Combining UNFOLD with SMASH or SENSE. In: Proceedings of the 9th Annual Meeting of ISMRM, Glasgow, Scotland, 2001.
20. Madore B, Fredrickson JO, Alley MT, Pelc NJ. A reduced field-of-view method to increase temporal resolution or reduce scan time in cine MRI. Magn Reson Med 2000;43:549–558.
21. Bracewell RN. The Fourier transform and its applications. 3rd ed. New York: McGraw-Hill; 1999.
22. Twieg DB. The k-trajectory formulation of the NMR imaging process with applications in analysis and synthesis of imaging methods. Med Phys 1983;10:610–621.
23. Press WH, Flannery BP, Teukolsky SA, Vetterling WT. Numerical recipes in C. Cambridge, UK: Cambridge University Press; 1988.
24. Fuderer M. The information content of MR images. IEEE Trans Med Imaging 1988;7:368–380.
25. Marseille GJ, De Beer R, Fuderer M, Mehlkopf AF, Van Ormondt D. Nonuniform phase-encode distributions for MRI scan time reduction. J Magn Reson Ser B 1996;111:70–75.
26. Cao Y, Levin DN, Yao L. Locally focused MRI. Magn Reson Med 1995;34:858–867.